Ciliopathy Protein Tmem107 Plays Multiple Roles in Craniofacial Development

Journal of Dental Research
2018, Vol. 97(1) 108–117

DOI: 10.1177/0022034517732538
journals.sagepub.com/home/jdr

P. Cela[1,2], M. Hampl[1,3], N.A. Shylo[4], K.J. Christopher[4], M. Kavkova[5], M. Landova[1,3], T. Zikmund[5], S.D. Weatherbee[4], J. Kaiser[5], and M. Buchtova[1,3]

Abstract

A broad spectrum of human diseases called ciliopathies is caused by defective primary cilia morphology or signal transduction. The primary cilium is a solitary organelle that responds to mechanical and chemical stimuli from extracellular and intracellular environments. Transmembrane protein 107 (TMEM107) is localized in the primary cilium and is enriched at the transition zone where it acts to regulate protein content of the cilium. Mutations in *TMEM107* were previously connected with oral-facial-digital syndrome, Meckel-Gruber syndrome, and Joubert syndrome exhibiting a range of ciliopathic defects. Here, we analyze a role of *Tmem107* in craniofacial development with special focus on palate formation, using mouse embryos with a complete knockout of *Tmem107*. *Tmem107*$^{-/-}$ mice were affected by a broad spectrum of craniofacial defects, including shorter snout, expansion of the facial midline, cleft lip, extensive exencephaly, and microphthalmia or anophthalmia. External abnormalities were accompanied by defects in skeletal structures, including ossification delay in several membranous bones and enlargement of the nasal septum or defects in vomeronasal cartilage. Alteration in palatal shelves growth resulted in clefting of the secondary palate. Palatal defects were caused by increased mesenchymal proliferation leading to early overgrowth of palatal shelves followed by defects in their horizontalization. Moreover, the expression of epithelial stemness marker SOX2 was altered in the palatal shelves of *Tmem107*$^{-/-}$ animals, and differences in mesenchymal SOX9 expression demonstrated the enhancement of neural crest migration. Detailed analysis of primary cilia revealed region-specific changes in ciliary morphology accompanied by alteration of acetylated tubulin and IFT88 expression. Moreover, *Shh* and *Gli1* expression was increased in *Tmem107*$^{-/-}$ animals as shown by in situ hybridization. Thus, TMEM107 is essential for proper head development, and defective TMEM107 function leads to ciliary morphology disruptions in a region-specific manner, which may explain the complex mutant phenotype.

Keywords: craniofacial anomalies, growth/development, mineralized tissue/development, orofacial clefts, cell signaling, oral pathology

Introduction

A defect in primary cilium morphology or function was revealed as one cause of cleft lip/palate formation (Tian et al. 2017). Primary cilia are small, microtubule-based projections from the cellular surface, covered by membrane with unique receptor and other signaling protein composition. Primary cilia were shown to be key organelles for the coordination of SHH, WNT, and PDGF signaling pathways (Haycraft et al. 2005; Schneider et al. 2005; Veland et al. 2009; Lee and Gleeson 2011). They play important roles in many developmental processes, such as neurulation, skeleton formation, and neural crest cell (NCC) migration (Chang et al. 2015), suggesting a key role for cilia during craniofacial development (Hu and Nelson 2011).

Mutations in genes encoding proteins important for cilia formation, structure, and function cause diseases called ciliopathies (Badano et al. 2006; Lee and Gleeson 2011). The number of syndromes classified as ciliopathies is still increasing, and it is estimated that one in a thousand children is born with a ciliary defect (Brugmann, Cordero, et al. 2010). Therefore, the identification of new ciliopathy genes is at the forefront of craniofacial research.

A primary cilium is composed of 9 pairs of microtubules, covered by a membrane and separated from the cytoplasm by transition fibers (Sorokin 1962). The transition zone in the proximal part of the cilium, distal to transition fibers, functions as a selective barrier, which regulates the movements of specific proteins between cilium and the cell body and therefore controls the signaling intensity (Hu and Nelson 2011).

[1]Institute of Animal Physiology and Genetics, CAS, Brno, Czech Republic
[2]Department of Physiology, University of Veterinary and Pharmaceutical Sciences, Brno, Czech Republic
[3]Department of Experimental Biology, Faculty of Sciences, Masaryk University, Brno, Czech Republic
[4]Department of Genetics, Yale University, School of Medicine, New Haven, CT, USA
[5]CEITEC—Central European Institute of Technology, Brno University of Technology, Brno, Czech Republic

A supplemental appendix to this article is available online.

Corresponding Author:
M. Buchtova, Institute of Animal Physiology and Genetics, v.v.i., Academy of Sciences of the Czech, Veveri 97, 602 00 Brno, Czech Republic.
Email: buchtova@iach.cz

Transmembrane protein 107 (TMEM107) is one of many factors located in the transition zone of cilia that control ciliary protein composition (Lambacher et al. 2016; Shylo et al. 2016). In mice, a point mutation in *Tmem107* (*Tmem107*^{schlei}) decreased cilia number and disrupted Hh signaling in several developing organs (Christopher et al. 2012).

In human patients with craniofacial abnormalities, whole-exome sequencing revealed a mutation in *TMEM107* (Iglesias et al. 2014). As of this writing, mutations in *TMEM107* have been described in patients diagnosed with oral-facial-digital syndrome (Lambacher et al. 2016; Shylo et al. 2016), Meckel-Gruber syndrome (Shaheen et al. 2015), and Joubert syndrome (Lambacher et al. 2016). All cases exhibited alterations in the number and/or length of cilia, confirming the critical, conserved role of TMEM107 protein in cilia formation. As all patients exhibited distinct craniofacial defects, we focused on detailed analyses of craniofacial structures in *Tmem107*-deficient mice to uncover developmental processes accompanying this ciliopathy.

Two mutant mouse alleles have been described for *Tmem107: Tmem107*^{schlei} and *Tmem107*^{tm1Lex} (Christopher et al. 2012). Here, we selected *Tmem107*^{tm1Lex} null mice, alternatively called *Tmem107*$^{-/-}$, for our analyses. This loss-of-function experimental approach enabled us to prove a critical role of this gene in palatogenesis and to test possible spatial-specific requirements for this protein in the palatal shelves.

Materials and Methods

Embryonic Material

Generation of the *Tmem107* null allele and recovery of the mouse line were previously described (Tang et al. 2010; Christopher et al. 2012). The details on the generation of the mutant can be found via the MMRRC strain information page (https://www.mmrrc.org/catalog/sds.php?mmrrc_id=32632). Briefly, all 5 exons of *Tmem107* were replaced with a targeting cassette, via homologous recombination, producing the null allele of *Tmem107*. The mouse line was reconstituted via in vitro fertilization and has been since crossed >10 generations onto the C57BL/6J background (Christopher et al. 2012). All mouse husbandry was performed in accordance with Yale's Institutional Animal Care and Use Committee guidelines. More details of the methodology used is included in the Appendix Methods.

Results

Tmem107$^{-/-}$ *Mice Exhibit Defects in Craniofacial Structures, Including Exencephaly, Eye Deficiencies, and Cleft Lip/Palate*

Wild-type (wt) and heterozygous animals of all observed stages showed normal external morphology (Appendix Table 1). In contrast, *Tmem107*$^{-/-}$ animals were affected by a broad spectrum of craniofacial defects, including the expansion of the facial midline (Fig. 1). Massive exencephaly with distinct abnormalities in head shape was observed in 30% animals of stage E12.5.

Microophthalmia or anophthalmia with optic nerve hypoplasia was observed in 67% of *Tmem107*$^{-/-}$ embryos (Fig. 1, Appendix Fig. 1, Appendix Table 1). In some cases, there was arrested eye development with only a small pigmented layer or lens pit that appeared to result from increased apoptosis and downregulation of the SOX2 progenitor marker (Appendix Fig. 1, data not shown).

Next, we observed defects in the rostral craniofacial area, where the snout was shorter and wider, resembling animals with altered SHH signaling (Brugmann, Allen, et al. 2010). Fourteen percent of individuals were affected with extensive cleft lip (Fig. 1, Appendix Table 1). In most cases (4/5), cleft lip was one-sided (right) and extended into the nasal cavity (Fig. 1, Appendix Fig. 2). Delay in palatal shelves growth was observed already in early stages of *Tmem107*$^{-/-}$ animals (Fig. 1J, L). The secondary palate remained open in *Tmem107*$^{-/-}$ animals during normal fusion stages between stages E14.5 and E15.5 (Fig. 1N, P) and also later at E16 (Appendix Fig. 2).

Moreover, the tongue was smaller, misshapen, and during palatal closure was observed located above palatal shelves (Appendix Fig. 2E, F; Appendix Figs. 4–6).

Abnormal Elevation and Orientation of Palatal Shelves Occur in Tmem107$^{-/-}$ *Animals*

Palatal processes are initiated as an outgrowth of the maxillary prominences at E12.5 in wild-type animals (Fig. 2A′). In contrast, most *Tmem107*$^{-/-}$ mice developed only indistinct medial outgrowth of palatal processes (Fig. 2E′, Appendix Fig. 3). Next, at E13.5, the anterior part of the secondary palate became oriented horizontally, while the posterior part of the secondary palate extended vertically downward in wild-type mice (Fig. 2B′–B″, Appendix Fig. 4). From this stage onward, palatal shelves were more expanded and the tongue was smaller in *Tmem107*$^{-/-}$ mice. The differences were distinct in the anterior and middle area of palatal shelves, while in the posterior area, shelves appeared more normal (Fig. 2F–F″, Appendix Fig. 4). By E14.5, anterior palatal shelves were misshapen or larger and oriented in the incorrect direction under the tongue in *Tmem107*$^{-/-}$ mice (Fig. 2G′–G″, Appendix Fig. 5). At E15.5, palatal shelves of *Tmem107*$^{-/-}$ mice were still vertically oriented in 1 case (Fig. 2H–H″, Appendix Fig. 6) or they grew horizontally but were not touching each other in the anterior part due to bilateral asymmetry (Appendix Fig. 6).

Tmem107$^{-/-}$ individuals of all analyzed stages also showed defects in the nasal area with the cavity expansions and rudimentary vomeronasal organ in several animals (Fig. 2F′, H′).

Skeletogenesis Is Delayed in Facial Membranous Bones of Tmem107$^{-/-}$ *Mice*

The onset of ossification in the palatal shelves of E15.5 *Tmem107*$^{-/-}$ animals (Fig. 3A–F, Appendix Movies 1, 2) was delayed as revealed by micro–computed tomography (CT)

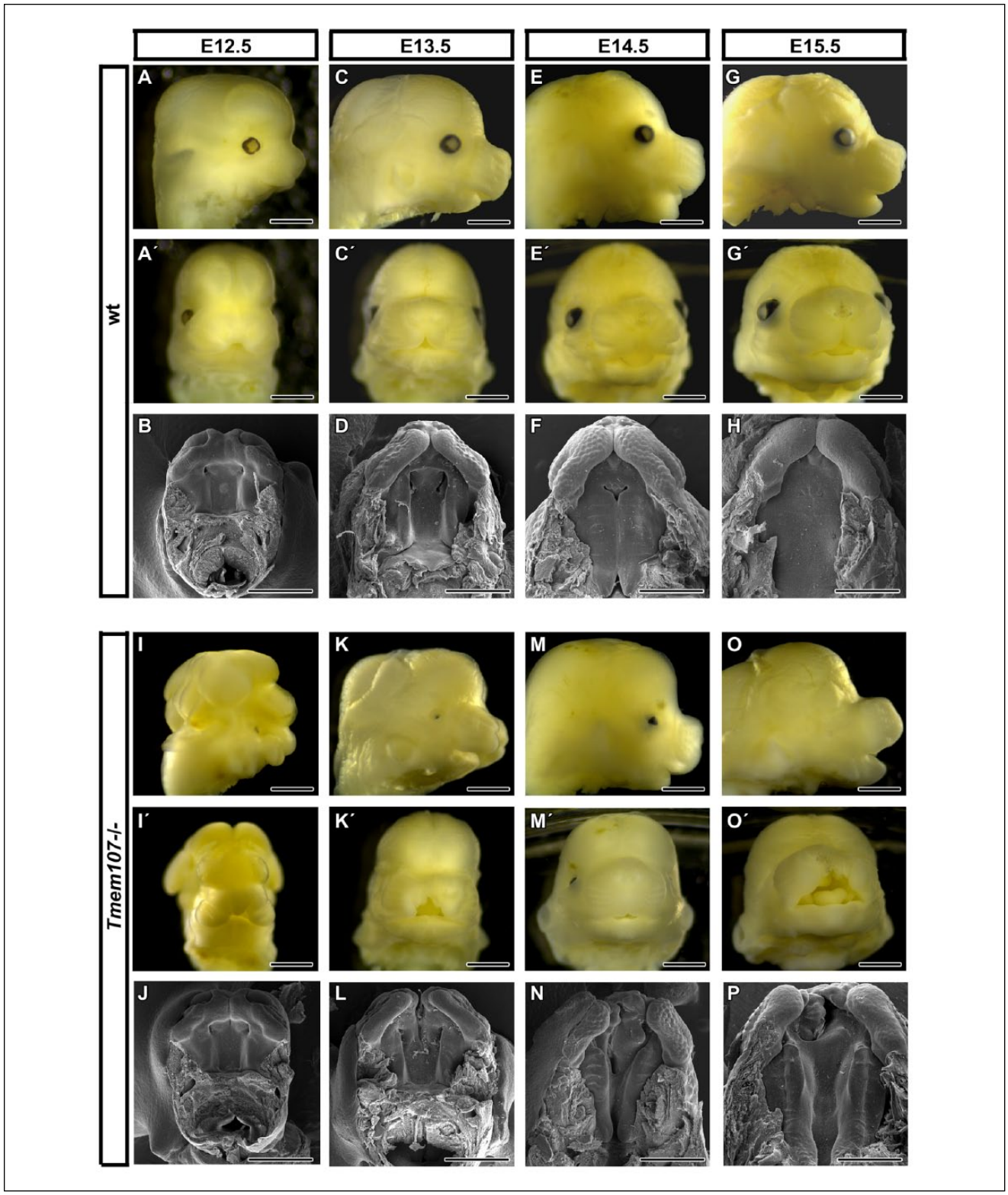

Figure 1. *Tmem107*$^{-/-}$ mutants display multiple gross morphological defects in craniofacial regions. E12.5, *Tmem107*$^{-/-}$ embryos (**I**, **I′**, **J**) exhibit exencephaly and altered morphology of the rostrum in comparison to wild-type (wt) animals (**A**, **A′**, **B**). At E13.5, *Tmem107*$^{-/-}$ mutants display cleft lip and palate (**K′**, **L**), in comparison to wt controls (**C**, **C′**, **D**). At E14.5, *Tmem107*$^{-/-}$ embryos display shorter snouts (**M**) together with cleft lip and palate (**N**) in contrast to wt animals (**E**, **F**). At E15.5, *Tmem107*$^{-/-}$ mutants show altered morphology of snout, together with cleft lip and palate (**O′**, **P**), compared to wt mice (**G**, **G′**, **H**). At all stages examined, *Tmem107*$^{-/-}$ embryos displayed reduced or absent eyes. Scale bar = 1 mm.

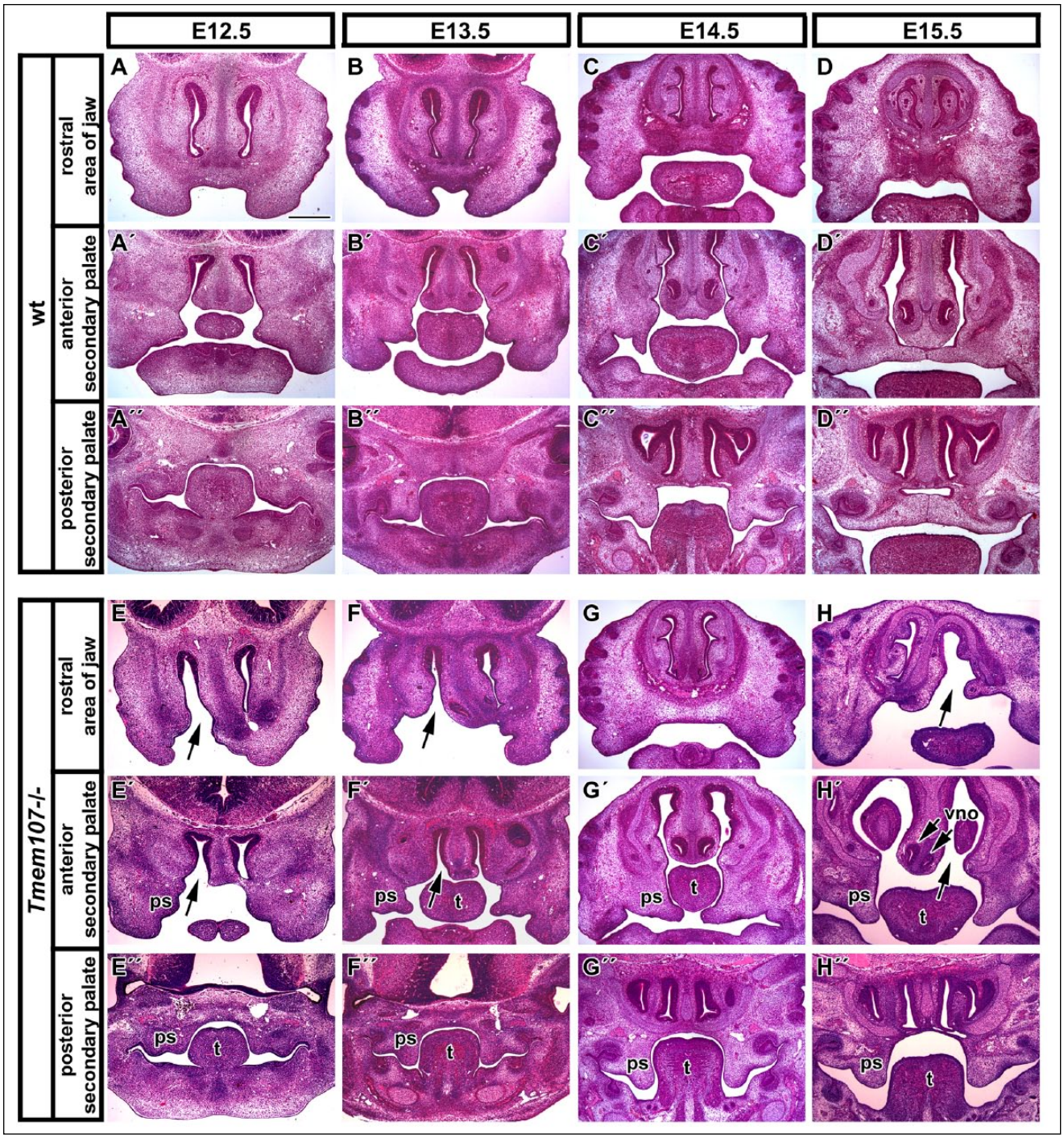

Figure 2. Palatogenesis is severely disrupted in *Tmem107*$^{-/-}$ mutants. Frontal sections of wild-type and *Tmem107*$^{-/-}$ embryos through different stages of palatogenesis. Rostral area of developing jaw of wt (**A**, **B**, **C**, **D**) and *Tmem107*$^{-/-}$ embryos with 1-sided cleft (black arrow) of the upper jaw (**E**, **F**, **G**, **H**). Anterior part of the secondary palate with physiological orientation of palatal shelves in wt animals (**A′**, **B′**, **C′**, **D′**). Anterior area of secondary palate in *Tmem107*$^{-/-}$ mutants with cleft phenotype (**E′**, **F′**, **G′**, **H′**). Abnormalities are the most obvious at E14.5 and E15.5 stages (G′, H′) when palatal shelves are thicker and oriented under the tongue. Posterior part of developing secondary palate in wt (**A″**, **B″**, **C″**, **D″**) and *Tmem107*$^{-/-}$ embryos with cleft palate (**E″**, **F″**, **G″**, **H″**). ps, palatal shelf; t, tongue; vno, vomeronasal organ. Scale bar = 500 µm.

analyses. The premaxillary ossification center was not visible, while maxillary, frontal, and parietal bones were smaller (Fig. 3A–F, Appendix Fig. 7). The ossification center of the mandibular bone was significantly shorter (Fig. 3A–F).

Next, we examined E16.5 skulls (n = 6) to follow later changes in bones and cartilages (Fig. 3G–N). Alizarin red and Alcian blue staining revealed that the zygomatic bone was mostly reduced (5/6), which correlated with eye defects.

Ossification of frontal, parietal, and interparietal bones was diminished (1/6 no sign of interparietal ossification). The nasal bone was smaller (2/6) or totally absent (4/6). Maxilla and premaxilla were abnormal or reduced in size in all embryos with premaxilla fusing across the ventral midline in half of the samples (3/6). Palatal shelves were ossified, but clefting was observed in all analyzed embryos (Fig. 3I–L, Appendix Fig. 7B). The mandible was shortened at this stage in all embryos (Fig. 2M, N). Meckel's cartilage was shorter in *Tmem107*$^{-/-}$ animals similarly to the mandible bone (Fig. 3M, N); however, we have not observed any dramatic changes in Meckel's cartilage morphology as has been described for other ciliopathies (Zhang et al. 2011).

Developmental abnormalities were also observed in craniofacial cartilages. Shape defects occurred in nasal septum cartilage with its enlargement of nasal septum or defects in vomeronasal cartilage formation (Fig. 3O–V′). Cartilage differentiation was initiated at the same stages in wild-type and *Tmem107*$^{-/-}$ animals as shown by SOX9 expression. Altered morphology of vomeronasal cartilage was observed accompanied with the fusion of their medial parts. The basisphenoid was abnormal with chondrogenesis as well as delayed ossification (6/6) (Appendix Figs. 7A, B and 8).

Tmem107 *Deletion Increases Proliferation in the Palatal Shelves*

Next, we investigated possible cellular changes to explain defects in palate formation. At the earliest analyzed stage (E12.5), we observed a lower proliferation in the tip area of the medial bulge on the maxillary prominence in contrast to wt controls (Appendix Fig. 9A–C). This pattern corresponds to altered intensity of outgrowth observed in these early mutant animals. However, analysis of mitotic index in the whole palatal prominence revealed slight upregulation of proliferation in *Tmem107*$^{-/-}$ mesenchyme (Appendix Fig. 9C). Later in development at E13.5 and E14.5, higher cell proliferation was also observed in the palatal shelves of *Tmem107*$^{-/-}$ mice, corresponding to morphological differences in palatal shelves of these animals (Appendix Fig. 9D–I). At the fusion stage (E15.5), few proliferating cell nuclear antigen (PCNA)-positive cells were observed surrounding the palatal seam in wt animals similarly, in *Tmem107*$^{-/-}$ mice, only a few positive cells were found in the mesenchyme while the tips of palatal shelves were almost completely PCNA negative (Appendix Fig. 9J–K′).

In contrast to the changes in cell proliferation, we observed only a few Terminal deoxynucleotidyl transferase dUTP nick end labeling (TUNEL)–positive cells at analyzed stages with their higher number in *Tmem107*$^{-/-}$ mice (Appendix Fig. 10A–K′). TUNEL-positive cells were seen especially in the ventral epithelium of palatal shelves in *Tmem107*$^{-/-}$ mice (Appendix Fig. 10B′, E′). At E15.5, TUNEL-positive cells were located in and surrounding the epithelial seam of wt mice (Appendix Fig. 10J, J′). In mutant mice, there were some apoptotic cells in the tip of palatal shelf as well as few cells in the underlying mesenchyme (Appendix Fig. 10K, K′).

Altered Expression of SOX Proteins Occurs in Tmem107$^{-/-}$ *Mice*

Proteins of the SOX family play key roles in cell fate determination as well as establishing and maintaining stem and progenitor cells in various tissues (Jo et al. 2014). Eleven members of the SOX family have been recently shown to be expressed in the palate (Watanabe et al. 2016). Here, we selected SOX2 and SOX9 for further analysis, as changes in the expression of SOX9 can reveal defects in neural crest cell migration and, in the case of the SOX2 progenitor cell, failure in palatal processes.

SOX2 is normally expressed in the oral epithelium during early palatogenesis, with the highest expression in the area located medially to the lingual side of tooth germ, while the most labial parts of the oral cavity are SOX2 negative (Fig. 4A). We have not observed differences in the anterior and posterior areas of palatal shelves and also any significant differences between *Tmem107*$^{-/-}$ and wt controls at E12.5 (Fig. 4A′, E′) or E13.5 (Fig. 4B′, F′). Later, at E14.5, wt animals have lower expression in the medial epithelium (Fig. 4C, C′). However, in *Tmem107*$^{-/-}$ mice, we did not observed downregulation of epithelial SOX2 expression in this area (Fig. 4G, G′). Significant downregulation of SOX2 expression was found in the tip of the *Tmem107*$^{-/-}$ palatal shelves much later in development at E15.5 (Fig. 4H, H′).

SOX9 can be found first in migrating cranial neural crest cells and later in the areas of cartilage and bone formation (Lee and Saint-Jeannet 2011). There were differences in expression pattern between wt and *Tmem107*$^{-/-}$ animals. At E12.5, SOX9-positive cells were located in deeper areas of the palatal mesenchyme (Fig. 4I, Q) with altered expression observed in *Tmem107*$^{-/-}$ animals (Fig. 4M, U). This upregulation in mice was even more apparent at E13.5. Posterior expression was located asymmetrically in the palatal shelves with higher expression in their medial part (Fig. 4R, V). At E14.5, SOX9-positive cells were located in the most distal tip of anterior palatal shelves and in the medial part of caudal palatal processes (Fig. 4K, S). Expression pattern was altered in *Tmem107*$^{-/-}$ animals, and SOX9 downregulation was observed

embryos (D) compared to wild-type (wt) (C). On frontal view, mandibular bones have a different shape and premaxillary bone is not well mineralized in *Tmem107*$^{-/-}$ mutants (F) in contrast to wt animals (E). Alcian blue/Alizarin red staining at E16.5 demonstrates delayed mineralization and altered morphology of frontal, parietal, and premaxillary bones in *Tmem107*$^{-/-}$ embryos (**H**, **J**) in comparison to wt (**G**, **I**). Palatine bones and palatal process of the maxillary bone are reduced in *Tmem107*$^{-/-}$ mutants (**L**) compared to wt (**K**). Mandibular bones are deformed in *Tmem107*$^{-/-}$ embryos (**N**) in contrast to wt animals (**M**). SOX9 expression in developing cartilages of interorbital septum and surrounding vomeronasal organ in wt animals through the palate development (**O–R**). Pattern of SOX9 expression is altered in *Tmem107*$^{-/-}$ mutants in correspondence to cartilage phenotype (**S–V**). Cartilages surrounding the vomeronasal organ exhibit altered shape; they were fused in midline (**S′**, **T′**, **U′**, **V′**) or missing (yellow arrow in T, T′). Nuclei are counterstained by DAPI (blue). fr, frontal bone; md, mandibular bone; mx, maxillary bone; ns, nasal septum; pl, palatal bone; pmx, premaxillary bone; pr, parietal bone; t, temporal bone; vnc, vomeronasal cartilage; vno, vomeronasal organ. Scale bar = 100 μm.

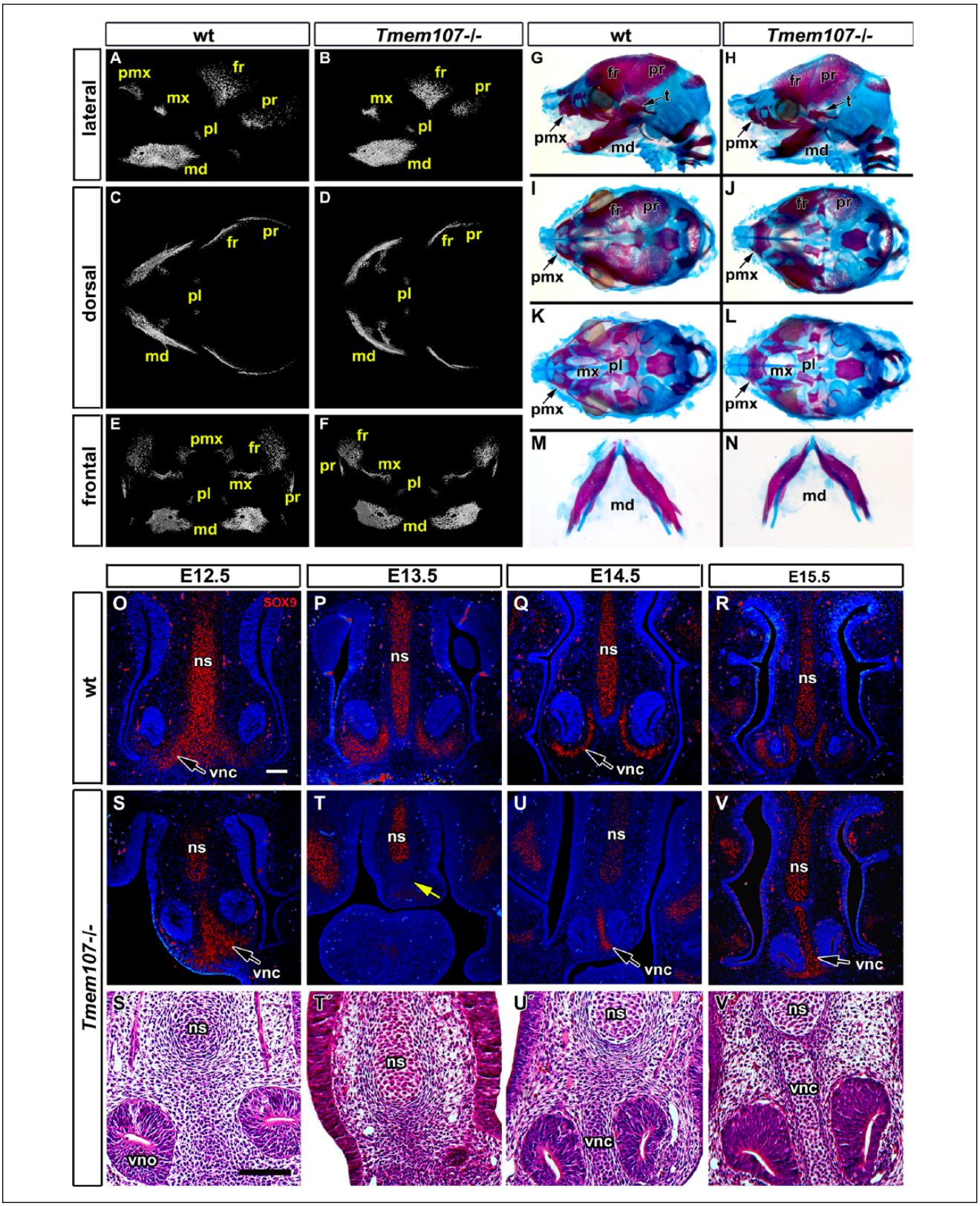

Figure 3. Reduced and delayed craniofacial skeletogenesis in *Tmem107*$^{-/-}$ embryos. Micro–computed tomography (CT) analysis of *Tmem107*$^{-/-}$ animals at E15.5 (**A–F**). Lateral view shows altered morphology and level of mineralization in maxillary, mandibular, and parietal bones in *Tmem107*$^{-/-}$ mutants and absence of the premaxillary bone (A, B). Ventral view reveals deformed mandibular bone and shorter frontal and parietal bones in *Tmem107*$^{-/-}$

in both analyzed areas (Fig. 4O, W). At E15.5, only a small amount of SOX9-positive cells was found in *Tmem107*$^{-/-}$ animals (Fig. 4P, X) in contrast to control animals (Fig. 4L, T).

Ciliary Morphology Disruptions Are Accompanied by Upregulated Expression of IFT88 and SHH Signaling

Previously, changes in number and morphology of primary cilia were observed in limb mesenchyme and the neural tube of *schlei* mice with a point mutation in *Tmem107* (Christopher et al. 2012). To test whether palatal cilia were disrupted in the full knockout of this gene, we analyzed cilia morphology on the palatal shelves surface in wt (Fig. 5A–B′) and *Tmem107*$^{-/-}$ mice (Fig. 5C–D′) by scanning electron microscopy (SEM). We observed numerous abnormal, very short, elongated or curly cilia in *Tmem107*$^{-/-}$ animals (Fig. 5D, D′, Appendix Fig. 11E–G′′′) resembling observations in *schlei* mutants (Christopher et al. 2012). Variability in cilia length was higher in *Tmem107*$^{-/-}$ animals than in controls, particularly in the anterior or middle areas of the palate (Appendix Fig. 11A). Occasionally, the enlargements or bulges were found in the most distal tip (Appendix Fig. 11E–G′′′).

To visualize mesenchymal cilia, we labeled them by acetylated α-tubulin (Fig. 5E–G′′, Appendix Figs. 12, 13). Mesenchymal cilia appeared to be elongated in *Tmem107*$^{-/-}$ animals (Fig. 5G–H′′). The analysis of acetylated α-tubulin expression revealed the higher expression of this protein in *Tmem107*$^{-/-}$ animals with the extensive variability of values in comparison to wt (Appendix Fig. 12E). The ciliary phenotypes identified in the mesenchyme by immunofluorescences resemble that observed on the epithelial cells via SEM (compare to Appendix Fig. 11A). In both controls and mutants, the length of mesenchymal cilia decreased as palate development progressed (Appendix Fig. 13; data not shown).

To analyze possible alteration in intraflagellar transport, we visualized the IFT88 protein on transversal histological sections through anterior and posterior areas of palatal shelves and double-labeled cilia with acetylated α-tubulin (Fig. 5E–H′′, Appendix Figs. 12, 13). Expression of IFT88 overlapped acetylated α-tubulin in cilia. In most cases, cilia with higher expression of acetylated α-tubulin exhibited also increased expression of IFT88 in *Tmem107*$^{-/-}$ animals.

To test if the altered morphology of primary cilia affected SHH signaling, we analyzed expression of *Shh* and downstream target *Gli1* by in situ hybridization on whole-mount palatal shelves (Fig. 5I–L). Increased expression of both genes was observed in the palatal ridges in *Tmem107*$^{-/-}$ mice (Fig. 5J, L).

Discussion

TMEM107 is a key factor for cilia formation and function. Here, we revealed an essential role for this protein during craniofacial development. To date, 6 human patients with 4 distinct *TMEM107* mutant alleles have been identified. These patients displayed variable phenotypes, and while none were specifically described as having cleft palate, they did show multiple craniofacial defects. All human patients with mutations in *TMEM107* described thus far have been either homozygotes (Shaheen et al. 2015; Lambacher et al. 2016; Shylo et al. 2016) or compound heterozygotes (Lambacher et al. 2016). Phenotypes observed in our null mice correspond largely with defects observed in human patients with homozygous mutation, and *Tmem107*$^{-/-}$ animals can serve as a model to study this ciliopathy. Moreover, parents of affected individuals (i.e., heterozygotes) have not been reported to have any abnormalities similar as we observed in our animals.

Cilia exhibit abnormal morphology and large variability in their length in *Tmem107* mutants, which likely modifies developmental signaling processes. Mice deficient in *Tmem107* resemble the phenotype of animals with altered SHH signaling, including exencephaly, polydactyly, disrupted modeling of the ventral neural tube, microophthalmia, and skeletal anomalies (Murdoch and Copp 2010). Moreover, TMEM107 protein function has been previously associated with SHH signaling during early embryogenesis (Christopher et al. 2012). Here, we showed that full truncation of this gene affects not just *Shh* expression but also downstream target *Gli1* in palatal ridges with the extension of their expression. We observed also expansion of the facial midline in our mice, which is typical for the disruption of SHH signaling (Brugmann, Allen, et al. 2010). In addition, *Tmem107*$^{-/-}$ animals showed abnormalities in head shape frequently accompanied with shorter snout and cleft lip and/or palate. In agreement with the craniofacial bones origin from the cranial neural crest and cranial mesoderm (Tobin et al. 2008), we found alteration of skeletogenesis similar to previously described ciliopathies.

Palatal cleft can be caused by variable developmental mechanisms from the failure of shelf initiation, intensity of proliferation or direction of shelf growth, insufficient horizontalization, or failure of their adhesion and disrupted palatal seam disintegration (Bush and Jiang 2012). We observed defects in secondary palate development from the earliest stages. Delayed growth of palatal shelves was observed in *Tmem107*$^{-/-}$-deficient mice at E12.5. However, later in development, they expanded largely, which resulted in incorrect orientation and position at the time of their elevation, leading to cleft formation. This expansion was accompanied by increased proliferation in the palatal mesenchyme. Similar increased proliferation leading to craniofacial defects, including cleft lip/palate, was observed in *Fuz*- and *Kif3a*-deficient mice (Zhang et al. 2011; Liu et al. 2014).

Tissue-specific response is characteristic of *Tmem107*$^{-/-}$ mice in the craniofacial area. Moreover, in the head, rostral structures of the oral cavity were more affected than caudal ones, and some structures with a known requirement for SHH signaling, such as hair, did not seem to be disrupted. It is possible that there is interaction with some tissue-specific genes such as members of the SOX family, which regulate different aspects of development, exhibit tissue-specific expression, and can play diverse function in individual organs such as cell fate

determination or maintenance of progenitor cells (Jo et al. 2014).

We observed strong SOX2 expression in the medial epithelium of palatal shelves in control animals, and this expression was downregulated in the lingual side and the tip of the shelves during their horizontalization. However, expression was not downregulated in the epithelium at the same stage in *Tmem107*$^{-/-}$ mice, indicating that epithelial cells are not able to control the expression changes at the right time. This is a critical step for shelf elevation, as shown previously in *Sox2*-deficient mice, which also have a delayed or failed shelf elevation (Langer et al. 2014).

The palatal shelves are composed of the mesenchyme derived mainly from neural crest cells (NCCs) (Ito et al. 2003). SOX9 is one of the markers of migrating NCCs (Spokony et al. 2002). In *Tmem107*$^{-/-}$ animals, we observed upregulation of SOX9 expression, associated with increased proliferation of mesenchymal cells. Our findings are consistent with previous experiments, where the loss of *Ift88* expression results in decreased NCC proliferation (Tian et al. 2017). As SOX9 is known to control primary cilia formation in bile ducts (Poncy et al. 2015) and to recruit GLI2 and GLI3 proteins during chondrocyte maturation to regulate transcription (Leung et al. 2011), it is probable that regulation of SOX9 through primary cilia function can affect stem cell status in craniofacial structures and delay their differentiation, resulting in overgrowth of palatal shelves.

Moreover, *Tmem107*$^{-/-}$ mice displayed microophthalmia or anophthalmia and optic nerve hypoplasia accompanied by loss of SOX2 expression in the eye area.

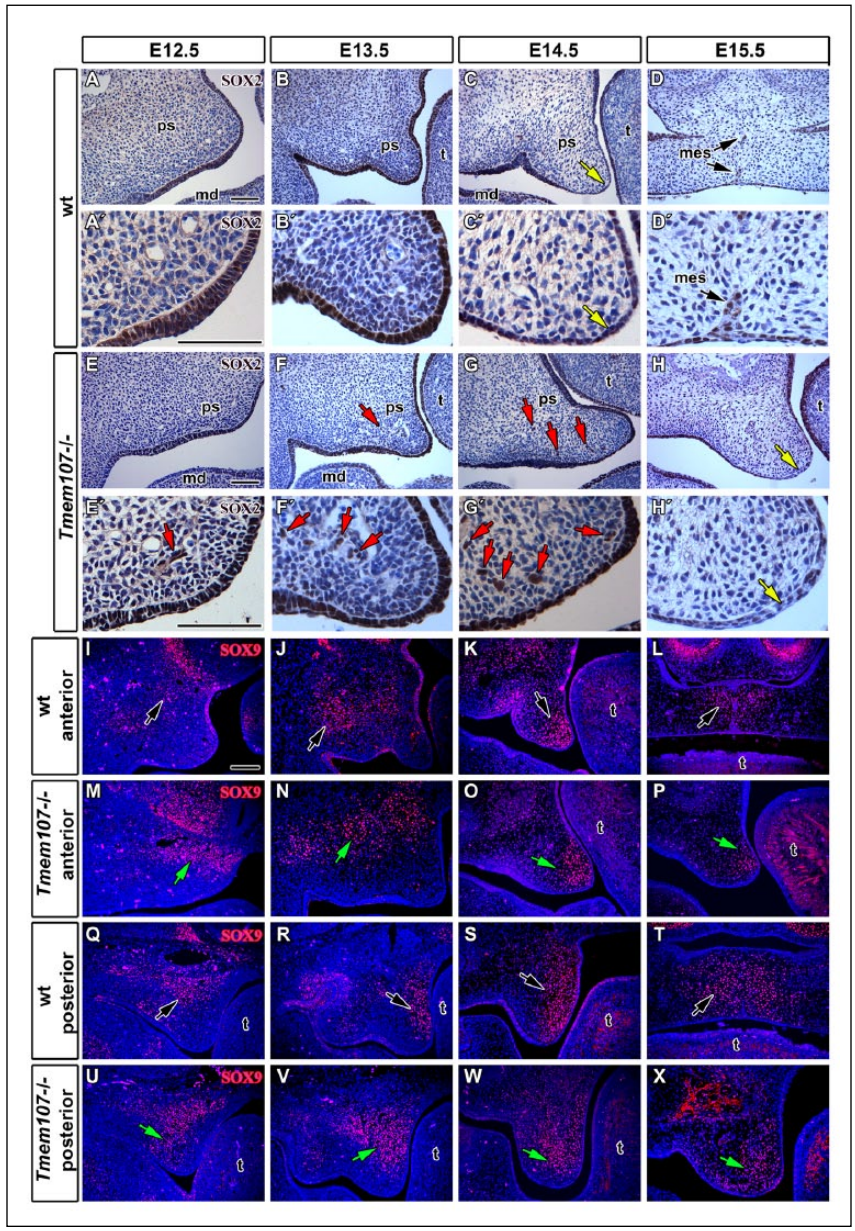

Figure 4. SOX expression shows distinct changes in *Tmem107*$^{-/-}$ palatal shelves. SOX2 expression (brown) is stronger in the palatal epithelium of E12.5 wt (**A**, **A′**) in comparison to *Tmem107*$^{-/-}$ mutants (**E**, **E′**). At E13.5, there are no significant differences in SOX2 expression between *Tmem107*$^{-/-}$ (**F**, **F′**) and wild-type (wt) embryos (**B**, **B′**). At E14.5, stronger SOX2 expression is detected in the tip of palatal shelves of *Tmem107*$^{-/-}$ mutants (**G**, **G′**), while downregulation of SOX2 occurs in the medial palatal epithelium of wt animals (**C**, **C′**). In E15.5 embryos, SOX2 expression is generally weaker in the oral epithelium in *Tmem107*$^{-/-}$ embryos (**H**, **H′**). In wt mice (**D**, **D′**), only residual expression is detected in the medial epithelial seam. Nuclei are counterstained by hematoxylin (blue). Several SOX2-positive cells were observed surrounding nerves and vessels (red arrows). In the anterior area of E12.5 palatal shelves, SOX9 expression (red) is detected in the mesenchyme dorsal to the main body of shelves in both mutant (**M**) and wt mice (**I**). In *Tmem107*$^{-/-}$ mutants (M), there is stronger SOX9 expression in comparison to wt (I). In the posterior area, SOX9 expression is located mainly in the dorsal mesenchyme in wt (**Q**). In *Tmem107*$^{-/-}$ (**U**), expression gradually increases from the ventral to dorsal mesenchyme of palatal shelves. In the anterior area of palatal shelves in E13.5 *Tmem107*$^{-/-}$ embryos (**J**), SOX9 expression is stronger in the mesenchyme, lateral to palatal shelves. In wt (**N**), there is only a small region of SOX9 expression. In the posterior area at E13.5, SOX9 expression is detected lingually in the mesenchyme, both in mutant (**V**) and wt (**R**) with higher expression in *Tmem107*$^{-/-}$ mutants. In the anterior area, at the E14.5 stage, SOX9 is expressed in the tip of the palatal plates (**K**, **O**), while in the posterior area, it is expressed particularly on the lingual side of palatal shelves (**S**). Altered pattern of expression is observed in *Tmem107*$^{-/-}$ palatal shelves (**W**). In the anterior area of E15.5 wt (**T**), SOX9 is expressed mainly in the midline of the fused palate (**L**), while in *Tmem107*$^{-/-}$ embryos (**P**), it is expressed just in the tip of the palatal mesenchyme inside its lingual side. In the posterior part of mice (T), SOX9 expression spreads more laterally from the midline, while in *Tmem107*$^{-/-}$ mutants (**X**), the strongest expression is detected in the lingual part of the palatal mesenchyme. Nuclei are counterstained by DAPI (blue). Changes in SOX9 expression are labeled by yellow arrows. md, mandible; ps, palatal shelve; mes, medial epithelial seam remnant; t, tongue. Scale bars = 100 µm.

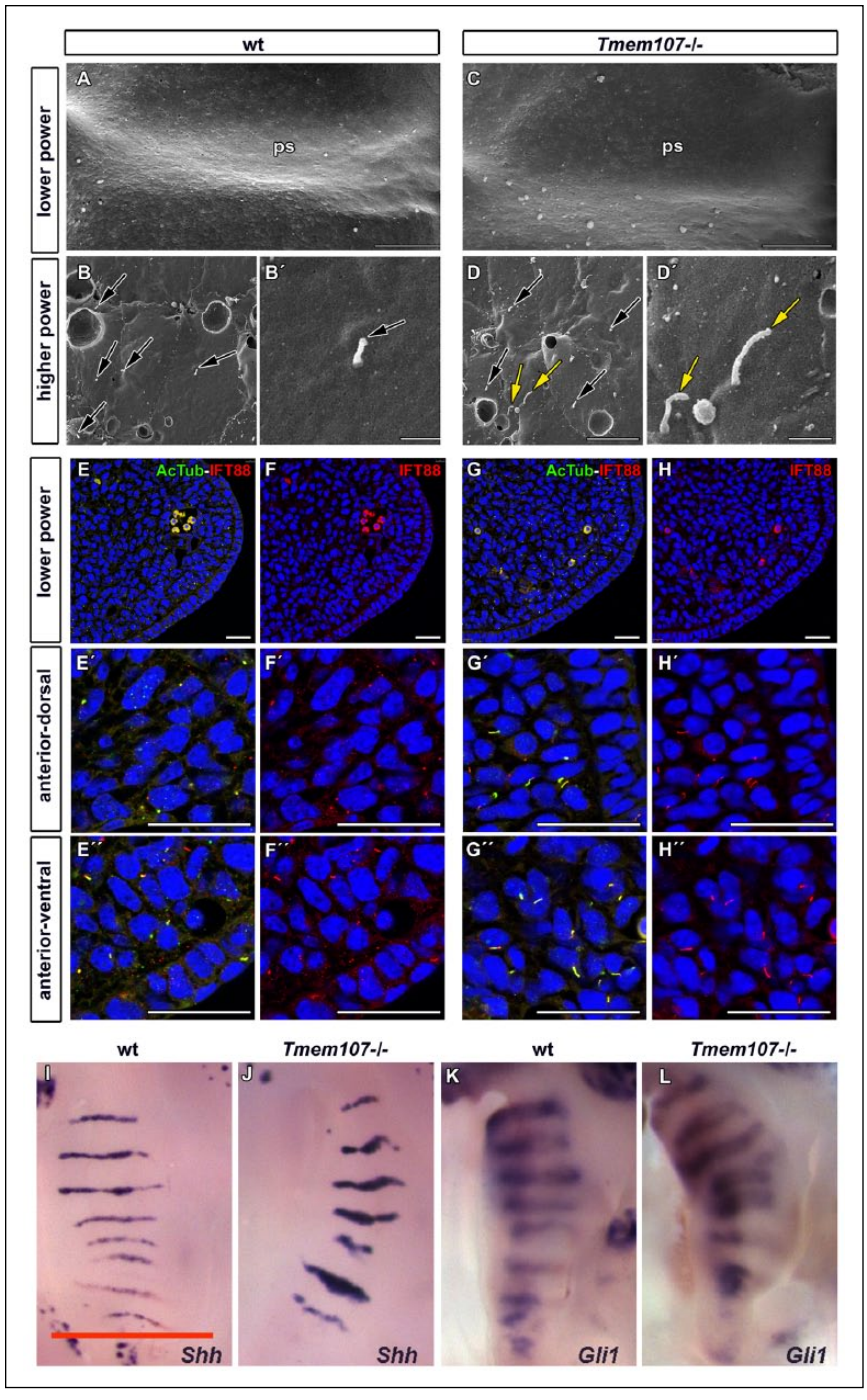

Figure 5. Cilia morphology, IFT88 expression, and Shh pathway signaling are altered in *Tmem107*$^{-/-}$ mutants. Low-magnification scanning electron microscope images of palatal shelves (ps) at E12.5 (**A**, **C**). Higher magnification examination of anterior, middle, and posterior areas of the palatal shelve surfaces revealed altered length and morphology of primary cilia in *Tmem107*$^{-/-}$ mutants (**D**, **D**′) compared to controls (**B**, **B**′). Numerous elongated, curly cilia or bulges on cilia tip (yellow arrows) or short cilia (black arrows) were detected. Scale bars for A and E = 100 µm, scale bar for B–D and F–H = 1 µm. Primary cilia labeled by α-acetylated tubulin appear longer and have altered shape in *Tmem107*$^{-/-}$ (**G′–H″**) compared to wild-type (wt) (**E′**, **F″**) in both ventral and dorsal parts of the anterior palatal shelves. IFT88 expression is more abundant in several cilia of *Tmem107*$^{-/-}$ mutants (D) in comparison to wt animals (B). Cilia were labeled with α-acetylated tubulin (green) and IFT88 (red) in developing palatal shelves (**A–D″**). Scale bar = 25 µm. Palatal views on E14.5 embryos exhibit higher expression of *Shh* and *Gli1* in the area of palatal ridges for both analyzed genes in *Tmem107*$^{-/-}$ mice (**J**, **L**) in comparison to littermate controls (**I**, **K**) as visualized by in situ hybridization. Scale bars = 1 mm.

In agreement with our results, a decrease in *Sox2* expression in zebrafish also resulted in eye and retina reduction (Chassaing et al. 2016). These results can be explained by the fact that SOX2 was shown to target multiple SHH effectors (Jeong and McMahon 2005). Direct interaction between SOX2 and PTCH proteins was previously confirmed by immunoprecipitation (Chassaing et al. 2016). The mechanism of how disrupted ciliary function affects SOX2 expression will be the basis of future studies.

In conclusion, we found that palatal clefts in *Tmem107*-deficient animals occur by dysregulation of mesenchymal proliferation and neural crest cell migration, leading to early overgrowth of palatal shelves followed by defects in their horizontalization. Therefore, further attention should be preferentially paid to downstream targets of SHH signaling, especially in the palatal mesenchyme.

Author Contributions

P. Cela, M. Hampl, contributed to data acquisition, analysis, and interpretation, drafted the manuscript; N.A. Shylo, contributed to data acquisition, analysis, and interpretation, critically revised the manuscript; S.D. Weatherbee, M. Buchtova, contributed to conception and design, critically revised the manuscript; M. Kavkova, M. Landova, T. Zikmund, contributed to data acquisition and analysis, drafted the manuscript; K.J. Christopher, contributed to data acquisition, critically revised the manuscript; J. Kaiser, contributed to data analysis, critically revised the manuscript. All authors gave final approval and agree to be accountable for all aspects of the work.

Acknowledgments

This work was supported by the Czech Science Foundation (14-37368G) and by the Ministry of Education, Youth and Sports of the Czech Republic (CZ.02.1.01/0.0/0.0/15_003/0000460) to M. Buchtova, National Institutes of Health grant R0AR059687 to S. Weatherbee, National Institute of General Medical Sciences (NIGMS) (training grant T32GM007499) and National Science Foundation Graduate Research Fellowships DGE-1122492 to N.A. Shylo, and DGE-0644492 to K.J. Christopher. MicroCT analysis was carried out under the project CEITEC 2020 (LQ1601) with

financial support from the Ministry of Education, Youth and Sports of the Czech Republic under the National Sustainability Programme II. The authors declare no potential conflicts of interest with respect to the authorship and/or publication of this article.

References

Badano JL, Mitsuma N, Beales PL, Katsanis N. 2006. The ciliopathies: an emerging class of human genetic disorders. Annu Rev Genomics Hum Genet. 7:125–148.

Brugmann SA, Allen NC, James AW, Mekonnen Z, Madan E, Helms JA. 2010. A primary cilia-dependent etiology for midline facial disorders. Hum Mol Genet. 19(8):1577–1592.

Brugmann SA, Cordero DR, Helms JA. 2010. Craniofacial ciliopathies: a new classification for craniofacial disorders. Am J Med Genet A. 152(12):2995–3006.

Bush JO, Jiang R. 2012. Palatogenesis: morphogenetic and molecular mechanisms of secondary palate development. Development. 139(2):231–243.

Chang CF, Schock EN, Attia AC, Stottmann RW, Brugmann SA. 2015. The ciliary baton: orchestrating neural crest cell development. Curr Top Dev Biol. 111:97–134.

Chassaing N, Davis EE, McKnight KL, Niederriter AR, Causse A, David V, Desmaison A, Lamarre S, Vincent-Delorme C, Pasquier L, et al. 2016. Targeted resequencing identifies PTCH1 as a major contributor to ocular developmental anomalies and extends the SOX2 regulatory network. Genome Res. 26(4):474–485.

Christopher KJ, Wang B, Kong Y, Weatherbee SD. 2012. Forward genetics uncovers Transmembrane protein 107 as a novel factor required for ciliogenesis and Sonic hedgehog signaling. Dev Biol. 368(2):382–392.

Haycraft CJ, Banizs B, Aydin-Son Y, Zhang Q, Michaud EJ, Yoder BK. 2005. Gli2 and Gli3 localize to cilia and require the intraflagellar transport protein polaris for processing and function. PLoS Genet. 1(4):e53.

Hu Q, Nelson WJ. 2011. Ciliary diffusion barrier: the gatekeeper for the primary cilium compartment. Cytoskeleton (Hoboken). 68(6):313–324.

Iglesias A, Anyane-Yeboa K, Wynn J, Wilson A, Truitt Cho M, Guzman E, Sisson R, Egan C, Chung WK. 2014. The usefulness of whole-exome sequencing in routine clinical practice. Genet Med. 16(12):922–931.

Ito Y, Yeo JY, Chytil A, Han J, Bringas P Jr, Nakajima A, Shuler CF, Moses HL, Chai Y. 2003. Conditional inactivation of Tgfbr2 in cranial neural crest causes cleft palate and calvaria defects. Development. 130(21):5269–5280.

Jeong J, McMahon AP. 2005. Growth and pattern of the mammalian neural tube are governed by partially overlapping feedback activities of the hedgehog antagonists patched 1 and Hhip1. Development. 132(1):143–154.

Jo A, Denduluri S, Zhang B, Wang Z, Yin L, Yan Z, Kang R, Shi LL, Mok J, Lee MJ, et al. 2014. The versatile functions of Sox9 in development, stem cells, and human diseases. Genes Dis. 1(2):149–161.

Lambacher NJ, Bruel AL, van Dam TJ, Szymanska K, Slaats GG, Kuhns S, McManus GJ, Kennedy JE, Gaff K, Wu KM, et al. 2016. TMEM107 recruits ciliopathy proteins to subdomains of the ciliary transition zone and causes Joubert syndrome. Nat Cell Biol. 18(1):122–131.

Langer L, Sulik K, Pevny L. 2014. Cleft palate in a mouse model of SOX2 haploinsufficiency. Cleft Palate Craniofac J. 51(1):110–114.

Lee JE, Gleeson JG. 2011. A systems-biology approach to understanding the ciliopathy disorders. Genome Med. 3(9):59.

Lee YH, Saint-Jeannet JP. 2011. Sox9 function in craniofacial development and disease. Genesis. 49(4):200–208.

Leung VY, Gao B, Leung KK, Melhado IG, Wynn SL, Au TY, Dung NW, Lau JY, Mak AC, Chan D, et al. 2011. SOX9 governs differentiation stage-specific gene expression in growth plate chondrocytes via direct concomitant transactivation and repression. PLoS Genet. 7(11):e1002356.

Liu B, Chen S, Johnson C, Helms JA. 2014. A ciliopathy with hydrocephalus, isolated craniosynostosis, hypertelorism, and clefting caused by deletion of Kif3a. Reprod Toxicol. 48:88–97.

Murdoch JN, Copp AJ. 2010. The relationship between sonic Hedgehog signaling, cilia, and neural tube defects. Birth Defects Res A Clin Mol Teratol. 88(8):633–652.

Poncy A, Antoniou A, Cordi S, Pierreux CE, Jacquemin P, Lemaigre FP. 2015. Transcription factors SOX4 and SOX9 cooperatively control development of bile ducts. Dev Biol. 404(2):136–148.

Schneider L, Clement CA, Teilmann SC, Pazour GJ, Hoffmann EK, Satir P, Christensen ST. 2005. PDGFRalphaalpha signaling is regulated through the primary cilium in fibroblasts. Curr Biol. 15(20):1861–1866.

Shaheen R, Almoisheer A, Faqeih E, Babay Z, Monies D, Tassan N, Abouelhoda M, Kurdi W, Al Mardawi E, Khalil MM, et al. 2015. Identification of a novel MKS locus defined by TMEM107 mutation. Hum Mol Genet. 24(18):5211–5218.

Shylo NA, Christopher KJ, Iglesias A, Daluiski A, Weatherbee SD. 2016. TMEM107 is a critical regulator of ciliary protein composition and is mutated in orofaciodigital syndrome. Hum Mutat. 37(2):155–159.

Sorokin S. 1962. Centrioles and the formation of rudimentary cilia by fibroblasts and smooth muscle cells. J Cell Biol. 15:363–377.

Spokony RF, Aoki Y, Saint-Germain N, Magner-Fink E, Saint-Jeannet JP. 2002. The transcription factor Sox9 is required for cranial neural crest development in Xenopus. Development. 129(2):421–432.

Tang T, Li L, Tang J, Li Y, Lin WY, Martin F, Grant D, Solloway M, Parker L, Ye W, et al. 2010. A mouse knockout library for secreted and transmembrane proteins. Nat Biotechnol. 28(7):749–755.

Tian H, Feng J, Li J, Ho TV, Yuan Y, Liu Y, Brindopke F, Figueiredo JC, Magee W 3rd, Sanchez-Lara PA, et al. 2017. Intraflagellar transport 88 (IFT88) is crucial for craniofacial development in mice and is a candidate gene for human cleft lip and palate. Hum Mol Genet. 26(5): 860–872.

Tobin JL, Di Franco M, Eichers E, May-Simera H, Garcia M, Yan J, Quinlan R, Justice MJ, Hennekam RC, Briscoe J, et al. 2008. Inhibition of neural crest migration underlies craniofacial dysmorphology and Hirschsprung's disease in Bardet-Biedl syndrome. Proc Natl Acad Sci U S A. 105(18):6714–6719.

Veland IR, Awan A, Pedersen LB, Yoder BK, Christensen ST. 2009. Primary cilia and signaling pathways in mammalian development, health and disease. Nephron Physiol. 111(3):39–53.

Watanabe M, Kawasaki K, Kawasaki M, Portaveetus T, Oommen S, Blackburn J, Nagai T, Kitamura A, Nishikawa A, Kodama Y, et al. 2016. Spatiotemporal expression of Sox genes in murine palatogenesis. Gene Expr Patterns. 21(2):111–118.

Zhang Z, Wlodarczyk BJ, Niederreither K, Venugopalan S, Florez S, Finnell RH, Amendt BA. 2011. Fuz regulates craniofacial development through tissue specific responses to signaling factors. PLoS One. 6(9):e24608.